Active control of sound radiation from a plate using a polyvinylidene fluoride volume displacement sensor

F. Charette[a] and A. Berry
G.A.U.S., Mechanical Engineering Department, Université de Sherbrooke, Sherbrooke, Québec J1K 2R1, Canada

C. Guigou
V.A.L., Mechanical Engineering Department, Virginia Polytechnic Institute and State University, Blacksburg, Virginia 24061-0238

(Received 18 April 1997; accepted for publication 19 November 1997)

This paper presents a new volume displacement sensor (made of shaped strips of PVDF film) and the experimental implementation of this sensor in an active control system. A design strategy for a PVDF sensor detecting the volume displacement induced by a vibrating 2D structure is presented. It is based on the modal representation of the plate response. It actually consists in designing a PVDF sensor, composed of several shaped PVDF strips bonded to the surface of the structure, in such a way that the output signal of the sensor is directly proportional to the volume displacement. The design methodology is based on the experimental measurements of the plate mode shapes (eigenfunctions) and is valid for any type of boundary conditions. The experimental implementation of such a volumetric sensor in an active control system is then presented. The experimental results obtained validates this new type of volume displacement sensor. © *1998 Acoustical Society of America.* [S0001-4966(98)00703-6]

PACS numbers: 43.40.Vn, 43.38.Fx [PJR]

INTRODUCTION

The two main strategies for actively controlling sound fields are active noise control (ANC) and active structural acoustic control (ASAC), first proposed by Fuller.[1,2] The ANC approach is based on controlling the acoustic field by using loudspeakers as acoustic secondary sources, while the ASAC approach directly modifies the response of the radiating structure by applying structural inputs as secondary sources, i.e., modal restructuring.[2] In general, the ASAC approach has been proved to require a smaller number of secondary sources for a global control of the acoustic field. Recently, piezoceramic actuators embedded in or bonded to the structure have been successfully used as structural secondary sources for ASAC applications.[3,4] These integrated-distributed actuators overcome many of the disadvantages of shakers.

In ASAC, the other component of prime importance is the error sensor, which defines the type of information to be minimized by the controller. Polyvinylidene fluoride (PVDF) materials have been suggested as error sensors in the active control of structural vibration,[5,6] and more recently in the active control of sound radiation.[7–10] In the latter case, the type of information measured on the structure by such sensors has to be carefully defined so that the minimization of this information effectively leads to a global attenuation of the sound field. In this instance, PVDF materials provide distributed sensors for which spatial filtering techniques can be applied by tailoring the sensor shape, in order to select, for example, the most efficient radiating modes in the structural response.

Since active control is most efficient at low frequencies, the development of appropriate sensors to be used in ASAC should be based on the low-frequency mechanisms of the sound radiation from vibrating structures. For planar radiators, it is well known that the sound radiation is directly related to the velocity distribution over the surface of that structure, for frequencies lower than the critical frequency. It was shown[11,12] that velocity distributions corresponding to certain modes, i.e., odd–odd or symmetric modes for simply supported and clamped boundary conditions, are the most efficient radiators. Therefore, the sensor to be designed should be able to mainly detect these well-radiating velocity distributions. A strategy originally investigated by Fuller *et al.*[13] is to detect only the supersonic (radiating) components of the structural wave number spectrum. Another approach is based on the ''radiation modes'' concept; it was shown[14,15] that the sound power can be written in terms of radiation modes, which correspond to the eigenvectors of the radiation impedance operator of the structure and radiate sound independently. Recently, Snyder *et al.*[10] have implemented the active control of sound radiation from a simply supported panel using PVDF film shaped in order to observe the radiation modes of the panel. The first and most radiating of these radiation modes was found to be the piston-type mode. Such a mode actually represents the monopole behavior of the structure and can be detected by measuring the net volume displacement over the surface of the structure. Based on this assumption, Rex and Elliott[16] developed a ''quadratically weighted strain integrating sensor,'' i.e., a quadratically

[a]F. Charette is currently working at the Vibration and Acoustics Laboratories (VAL) of Virginia Polytechnic Institute & State University.

weighted sensor measuring the volume velocity of the structure. This sensor can be implemented in practice in the form of a piezoelectric cable or an optical fiber bonded on or embedded in the structure. Using the same approach, Johnson and Elliott[17] showed that the volume velocity of a two-dimensional structure can be measured by quadratically weighting the sensitivity or the thickness of an extended PVDF sensor covering the whole surface of the structure. This solution being unrealistic in practice, it was approximated by shaping the sensor into quadratic or rectangular strips.[18] They successfully implemented active control of volume displacement using such sensor on a plate and observed significant reductions in the sound radiations. However, the disadvantage of their sensor design is that it has to cover the whole plate surface, which may not be available in many applications. Recently, Guigou *et al.*[8] have successfully implemented active control of volume displacement in the case of flexural beams, by using a single shaped PVDF strip, and they observed significant attenuation of the radiated sound field. The shape of the PVDF strip was based on the mode shapes (eigenfunctions) of the beam. This last work provides the basis of the present investigation.

The objective of this paper is to extend the concepts of the abovementioned paper in the case of 2D structures. The implementation of an extended, shaped PVDF sensor as a volume displacement sensor is discussed in the case of a rectangular panel with arbitrary boundary conditions; the sensor shape is shown to be independent of the frequency and type of excitation. Moreover, the strategy of minimizing the volume velocity keeps the control architecture very simple (single input control system). Experimental results of the volume displacement sensor and its use in an active control system are presented and discussed.

I. VOLUME DISPLACEMENT PVDF SENSOR

A. Description of the system considered

The mechanical system studied in this paper consists of a rectangular clamped plate on which two piezoelectric actuators are bonded; see Fig. 1. A piezoelectric actuator is composed of two identical colocated piezoceramic patches on each side of the plate. The piezoceramic patches are assumed to be perfectly bonded to the plate surface. A symmetric actuation (pure flexion) is induced in the plate when the two piezoceramic patches are driven 180° out of phase.[2] Here, one of the piezoelectric actuators is used to induce the unwanted vibration (i.e., primary actuator) while the second actuator is the control (i.e., secondary) actuator. The plate dimensions and material properties are described in Table I. The piezoceramic actuators characteristics and locations are given in Table II.

TABLE I. Properties of the clamped plate.

L_x^{pl}	50.0 cm
L_y^{pl}	39.8 cm
L_z^{pl}	3.15 mm
Young's modulus (E)	6.5×10^{10} Pa
Density (ρ)	2800 kg/m^3

The total transverse displacement of the plate under the action of the primary and secondary actuators can be written as a linear combination of modes,

$$w(x,y)=\sum_{i=1}^{l}\hat{W}_i\Psi_i(x,y), \tag{1}$$

where $\hat{W}_i$ is the modal amplitude and $\Psi_i(x,y)$ is the ith eigenfunction. The modal sum in Eq. (1) is truncated to ''I'' modes.

B. Experimentally determined eigenfunctions

The design of the volume displacement sensor starts with the determination of the plate eigenfunctions. In this work, these eigenfunctions are determined experimentally, even though theoretical approximations are available in the case of clamped plate. The experimental determination of the eigenfunctions can lead to a better representation of a particular ''real'' (i.e., experimental) plate displacement, since it takes into account the imperfections in the boundary conditions, plate material, external loading, etc. Furthermore, using experimentally measured eigenfunctions would be natural for more complex plates for which no theoretical approximations are easily available.

The plate was excited between 100 and 500 Hz, using the primary PZT actuator, in order to obtain its modal characteristics. A Bruel & Kjaer analyser was used to measure the transfer function between the velocity signal from a laser vibrometer [at a total of 144 (12×12) regularly spaced measurement points] and the excitation signal. The modal analysis STAR SYSTEMS V5.0 package was then used to process the data. This software uses a frequency domain curve-fitting analysis to determine the modal characteristics. The experimental mode shapes $\Psi_i(x,y)$ are then represented as a combination of polynomial trial functions,

$$\Psi_i(x,y)=\sum_{p=0}^{P-1}\sum_{q=0}^{Q-1}A_{i,pq}\left(\frac{x}{L_x^{pl}}\right)^p\left(\frac{y}{L_y^{pl}}\right)^q. \tag{2}$$

Such trial functions are very general and may be used for plates with arbitrary boundary conditions. In order to determine the unknown coefficients $A_{i,pq}$ of a mode shape, the following system of equations has to be solved for each mode ''i,''

$$[\varphi_{mnpq}]\{A_{i,pq}\}=\{w_{i,mn}\}. \tag{3}$$

The vector $\{w_{i,mn}\}$ contains the ith modal displacement of the mnth measurement point as provided by the STAR SYSTEMS package. The vector $\{w_{i,mn}\}$ thus contains 144 elements. The coefficients of the matrix $[\varphi_{mnpq}]$ are given by

$$\varphi_{mnpq}=\left(\frac{x_m}{L_x^{pl}}\right)^p\left(\frac{y_n}{L_y^{pl}}\right)^q, \tag{4}$$

where x_m and y_n are the positions of the mnth measurement point.

Reasonably small values of P and Q in Eq. (2) are sufficient to reconstruct the first few modes of the plate. Consequently, the values of P and Q are usually smaller than the

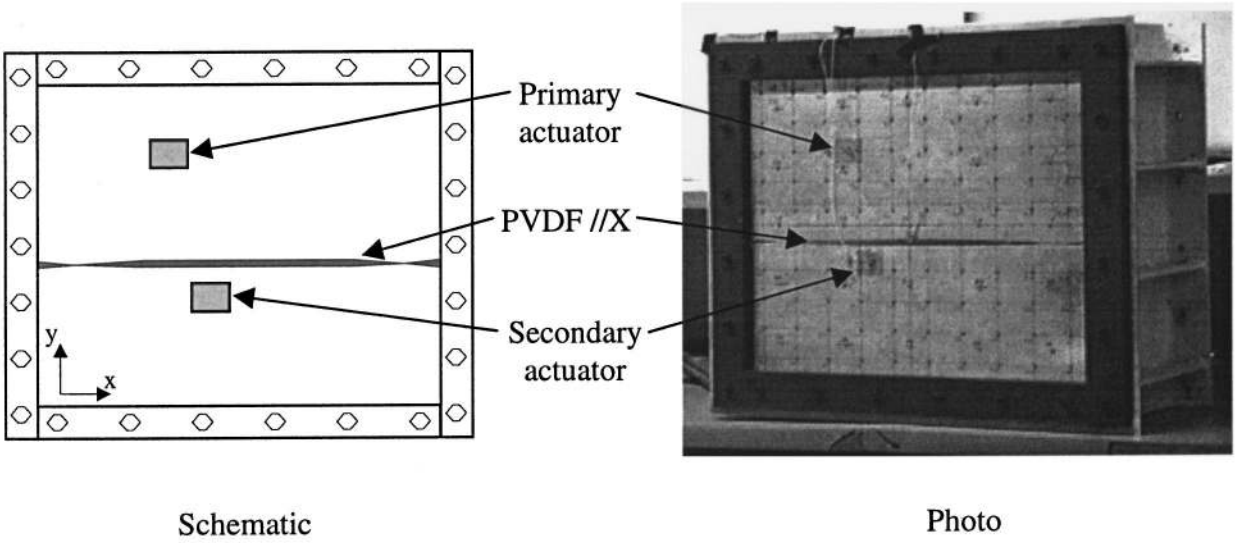

(a) Front of the plate

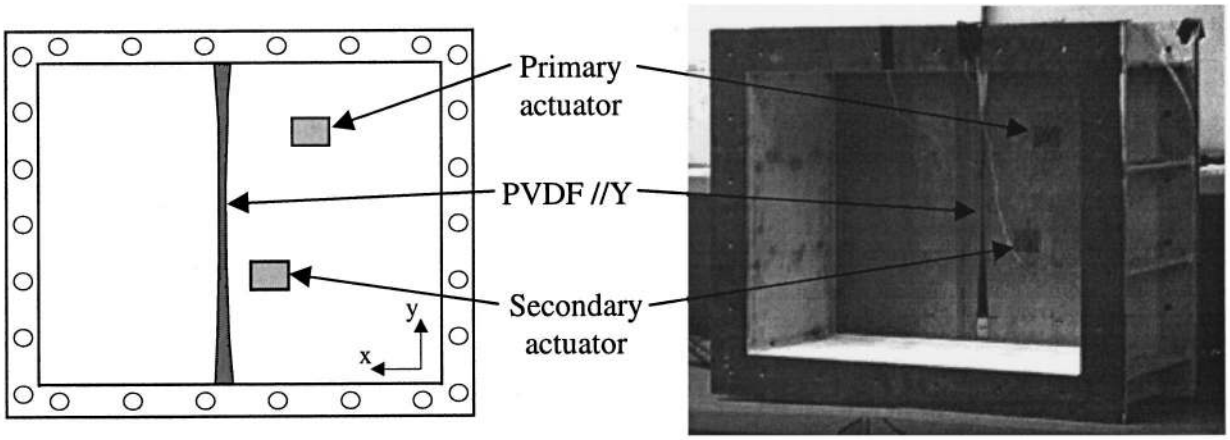

(b) Back of the plate

FIG. 1. Clamped plate studied.

number of measurement points in each direction of the plate and the linear system represented by Eq. (3) is overdetermined. Therefore, a least mean square technique is used and the following system has to be solved,

$$[\varphi_{mnpq}]^T[\varphi_{mnpq}]\{A_{i,pq}\}=[\varphi_{mnpq}]^T\{w_{i,mn}\}. \tag{5}$$

The superscript T indicates the transpose operator. A criterion must be used to evaluate the accuracy of the polynomial approximation obtained. The criterion suggested by Gerald and Wheatley[19] is to increase the degree of the approximation polynomials until a statistically significant decrease in the variance of the approximation error is obtained. The variance of the error is defined as

$$\chi_i^2=\frac{\Sigma_{m=1}^{M}\Sigma_{n=1}^{N}(\Psi_i(x_m,y_n)-w_{i,mn})^2}{M\cdot N-P\cdot Q-1}, \tag{6}$$

where ''M'' and ''N'' are the total number of measuring points in the x and y directions, respectively. Thus the orders ''P'' and ''Q'' of the approximation polynomials are selected independently for each mode ''i'' using Eq. (6) as criterion.

C. Structural volume displacement of a plate

In the present work, the cost function considered for the active control system is the structural volume displacement

TABLE II. Ceramic piezo-characteristics.

	Primary	Secondary
L_x^{pz}	3.81 cm	3.81 cm
L_y^{pz}	3.18 cm	3.18 cm
L_z^{pz}	0.19 mm	0.19 mm
Pos. of the center along the x axis	16.0 cm	19.0 cm
Pos. of the center along the y axis	30.0 cm	15.0 cm
Young's modulus (E_{11})	6.3×10^{10} Pa	6.3×10^{10} Pa
Density (ρ)	7750 kg/m^3	7750 kg/m^3

of the plate. The structural volume displacement is defined as the integral of the transverse displacement over the surface of the plate,

$$D=\int_0^{L_y^{pl}}\int_0^{L_x^{pl}} w(x,y)dx\ dy. \tag{7}$$

Introducing Eqs. (1) and (2) into Eq. (7) and performing the double integration yields the volume displacement of the plate, which can be written in matrix form as

$$D=L_x^{pl}L_y^{pl}\langle\hat{W}_i\rangle[A_{i,pq}]\{D_{pq}\}. \tag{8}$$

The dimensions of the matrix $[A_{i,pq}]$ are "I" rows by "$P\times Q$" columns. Each row of the matrix $[A_{i,pq}]$ contains the coefficients of a given eigenfunctions $\Psi_i(x,y)$ over the polynomial trial functions. The line vector $\langle\hat{W}_i\rangle$ contains the modal amplitudes. The components of the column vector $\{D_{pq}\}$ are simply given by $1/[(p+1)(q+1)]$.

The volume velocity of the plate is simply Eq. (8) multiplied by $j\omega$ as harmonic excitation is assumed. Thus for pure tone excitation, it is equivalent to minimize the volume velocity or the net volume displacement. The strategy of using the volume displacement as a cost function for an active control system have been shown previously[8,15,18] to be very efficient to reduce sound radiation in the low-frequency range (i.e., $k_0L\ll1$, k_0 is the wave number in air, and L is the characteristic dimension of the structure).

D. Design of a volume displacement sensor using shaped PVDF film

The charge response of an arbitrarily shaped strip of PVDF sensor applied to a two-dimensional structure has been derived by Lee *et al.*[5] It was shown that the charge response of the sensor is a function of the integral of the strain over the surface of application and is expressed as

$$q=-\frac{L_z^{pl}+L_z^s}{2}\int_0^{L_y^{pl}}\int_0^{L_x^{pl}}\left[e_{31}\frac{\partial^2w(x,y)}{\partial x^2}+e_{32}\frac{\partial^2w(x,y)}{\partial y^2}+2e_{36}\frac{\partial^2w(x,y)}{\partial x\partial y}\right]\cdot F(x,y)\cdot dx\ dy, \tag{9}$$

where L_z^{pl} and L_z^s are, respectively, the plate thickness and PVDF sensor thickness. The e_{ij} are the PVDF sensor stress/charge coefficients. It is assumed that no skew angle is associated with the polarization of the PVDF film used in this study, $e_{36}=0$. The function $F(x,y)$ represents the variation of the film sensitivity with the position on the surface of application. In practice, this variation of sensitivity is more easily achieved by shaping the PVDF film as described in the following.

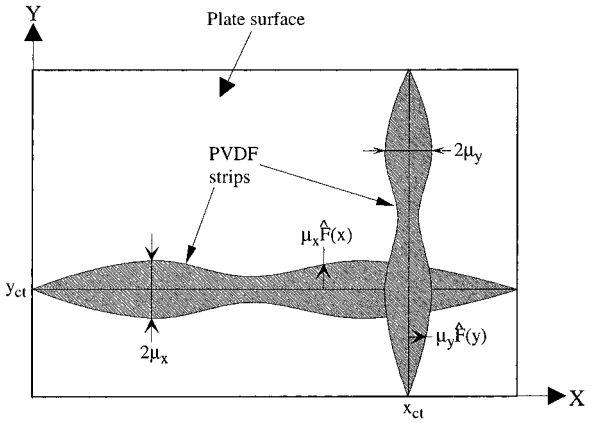

FIG. 2. Top view of the finite plate with a typical shaped PVDF strips configuration.

First, consider a single PVDF strip parallel to the x direction of the plate, whose center line is located at $y=y_{ct}$, as shown in Fig. 2. The maximum width of the strip is noted $2\mu_x$, and the width at the position x is $2\mu_x\hat{F}(x)$, where $\hat{F}(x)$ is a function varying between -1 and $+1$. Negative values of $\hat{F}(x)$ correspond to an inversion of the PVDF film polarity. It is assumed that the strip axis coincides with the direction of maximum stress/charge coefficient e_{31}. It is desired to find the output response of this strip when the function $\hat{F}(x)$ is given by

$$\hat{F}(x)=\sum_{r=0}^{R-1}\hat{\alpha}_r\left(\frac{x}{L_x^{pl}}\right)^r. \tag{10}$$

In this case, the charge response of the PVDF strip can be written as

$$q_x=-\frac{L_z^{pl}+L_z^s}{2}\int_0^{L_x^{pl}}\int_{y_{ct}-\mu_x\hat{F}(x)}^{y_{ct}+\mu_x\hat{F}(x)}\left[e_{31}\frac{\partial^2w(x,y)}{\partial x^2}+e_{32}\frac{\partial^2w(x,y)}{\partial y^2}\right]dy\,dx. \tag{11}$$

Introducing Eqs. (1) and (2) into Eq. (11) and integrating with respect to the variable y leads to

$$q_x=-\frac{L_z^{pl}+L_z^s}{2}\sum_{i=1}^{l}\hat{W}_i\sum_{p=0}^{P-1}\sum_{q=0}^{Q-1}A_{i,pq}\int_0^{L_x^{pl}}\left\{\frac{e_{31}p(p-1)L_y^{pl}}{(q+1)(L_x^{pl})^2}\times\left(\frac{x}{L_x^{pl}}\right)^{p-2}\cdot\left(\frac{y_{ct}}{L_y^{pl}}\right)^{q+1}\cdot\left[\left(1+\frac{\mu_x\hat{F}(x)}{y_{ct}}\right)^{q+1}-\left(1-\frac{\mu_x\hat{F}(x)}{y_{ct}}\right)^{q+1}\right]+\frac{e_{32}qL_y^{pl}}{(L_y^{pl})^2}\left(\frac{x}{L_x^{pl}}\right)^{p}\cdot\left(\frac{y_{ct}}{L_y^{pl}}\right)^{q-1}\cdot\left[\left(1+\frac{\mu_x\hat{F}(x)}{y_{ct}}\right)^{q-1}-\left(1-\frac{\mu_x\hat{F}(x)}{y_{ct}}\right)^{q-1}\right]\right\}dx. \tag{12}$$

At this point, it is necessary to introduce a simplifying assumption before integrating along the strip axis: If the width μ_x of the strip is small enough such that $|\mu_x \hat{F}(x)/y_{ct}| \ll 1$ then

$$\left(1+\frac{\mu_x \hat{F}(x)}{y_{ct}}\right)^{q+1} \approx 1+\frac{(q+1)\mu_x \hat{F}(x)}{y_{ct}} + \frac{q(q+1)}{2}\left(\frac{\mu_x \hat{F}(x)}{y_{ct}}\right)^2. \tag{13}$$

Similar assumptions are made for

$$\left(1-\frac{\mu_x \hat{F}(x)}{y_{ct}}\right)^{q+1}, \quad \left(1+\frac{\mu_x \hat{F}(x)}{y_{ct}}\right)^{q-1},$$

and

$$\left(1-\frac{\mu_x \hat{F}(x)}{y_{ct}}\right)^{q-1}.$$

Inserting these approximations into Eq. (12) and performing the integration along the x axis, the charge of the PVDF strip parallel to the x axis can be written in matrix form as

$$q_x = -\frac{L_z^{pl}+L_z^s}{2}\langle \hat{W}_i \rangle [A_{i,pq}][T1_{pq,r}]\{\hat{\alpha}_r\}, \tag{14}$$

where $\{\hat{\alpha}_r\}$ is the vector of the shape coefficients of the PVDF strip. The coefficients of the matrix $[T1_{pq,r}]$ are given by

$$T1_{pq,r} = \frac{2\mu_x e_{31} p(p-1)}{L_x^{pl}(p+r-1)}\left(\frac{y_{ct}}{L_y^{pl}}\right)^q + \frac{2\mu_x L_x^{pl} e_{32} q(q-1)}{(L_y^{pl})^2(p+r+1)}\left(\frac{y_{ct}}{L_y^{pl}}\right)^{q-2}. \tag{15}$$

Similarly, for a PVDF strip parallel to the y direction at $x = x_{ct}$, with a maximum width $2\mu_y$ (see Fig. 2) and a shape described by

$$\hat{F}(y) = \sum_{s=0}^{S-1} \hat{\beta}_s \left(\frac{y}{L_y^{pl}}\right)^s, \tag{16}$$

the charge response is given by

$$q_y = -\frac{L_z^{pl}+L_z^s}{2}\sum_{i=1}^{l}\hat{W}_i \sum_{p=0}^{P-1}\sum_{q=0}^{Q-1} A_{i,pq}\int_0^{L_y^{pl}} \left\{ \frac{e_{31} q(q-1) L_x^{pl}}{(p+1)(L_y^{pl})^2} \times \left(\frac{y}{L_y^{pl}}\right)^{q-2} \cdot \left(\frac{x_{ct}}{L_x^{pl}}\right)^{p+1} \cdot \left[\left(1+\frac{\mu_y \hat{F}(y)}{x_{ct}}\right)^{p+1} - \left(1-\frac{\mu_y \hat{F}(y)}{x_{ct}}\right)^{p+1} \right] + \frac{e_{32} p}{L_x^{pl}} \left(\frac{y}{L_y^{pl}}\right)^q \cdot \left(\frac{x_{ct}}{L_x^{pl}}\right)^{p-1} \cdot \left[\left(1+\frac{\mu_y \hat{F}(y)}{x_{ct}}\right)^{p-1} - \left(1-\frac{\mu_y \hat{F}(y)}{x_{ct}}\right)^{p-1} \right] \right\} dy. \tag{17}$$

Using approximations similar to Eq. (13) for the terms $(1+[\mu_y \hat{F}(y)/x_{ct}])^{p+1}$, etc., and performing the integration along the y axis, the charge of the PVDF strip parallel to the y axis can be written in matrix form as

$$q_y = -\frac{L_z^{pl}+L_z^s}{2}\langle \hat{W}_i \rangle [A_{i,pq}][T2_{pq,s}]\{\hat{\beta}_s\}, \tag{18}$$

where

$$T2_{pq,s} = \frac{2\mu_y e_{31} q(q-1)}{L_y^{pl}(q+s-1)}\left(\frac{x_{ct}}{L_x^{pl}}\right)^p + \frac{2\mu_y L_y^{pl} e_{32} p(p-1)}{(L_x^{pl})^2(q+s+1)}\left(\frac{x_{ct}}{L_x^{pl}}\right)^{p-2}. \tag{19}$$

The total output charge $q = q_x + q_y$ written in matrix form is

$$q = -\frac{L_z^{pl}+L_z^s}{2}\langle \hat{W}_i \rangle \{[A_{i,pq}][T1_{pq,r}]\{\hat{\alpha}_r\} + [A_{i,pq}][T2_{pq,s}]\{\hat{\beta}_s\}\}. \tag{20}$$

It is required that the sum of the output charges be proportional to the net volume displacement of the plate. In this case, the sensor formed by the 2 PVDF strips is a volume displacement sensor. This requirement allows the unknown coefficients $\hat{\alpha}_r$ and $\hat{\beta}_s$ of the strip shapes to be determined. Equating Eqs. (8) and (20) row by row implies that the modal volume displacements of the plate are equal to the modal charge response of the sensor, which ensures that the sensor is independent of the frequency; this yields

$$-\frac{L_z^{pl}+L_z^s}{2}\{[A_{i,pq}][T1_{pq,r}]\{\hat{\alpha}_r\} + [A_{i,pq}][T2_{pq,s}]\{\hat{\beta}_s\}\} = L_x^{pl} L_y^{pl}[A_{i,pq}]\{D_{pq}\}. \tag{21}$$

Equation (21) forms a system of I linear equations to be solved for the $R+S$ unknown coefficients $\hat{\alpha}_r$ and $\hat{\beta}_s$. A unique solution is obtained if $R+S=I$, I being the total number of modes considered in the plate response. So, this uniqueness condition relates the total number of modes to the order of the polynomials used to shape the strips of PVDF. Note that high order polynomials yield complicated shapes of PVDF strips (with possibly many zeros, thus many polarity changes) implying difficulties in experimental implementation. Therefore, when the number of modes I considered is large, it is worthwhile to consider more than one strip in the x and/or y directions. Adding strips on the plate allows the order of the shape polynomials to be kept small for each strip. Equation (21) can easily be extended to consider more than one strip in the x or y direction. It is also interesting to note that since matrix $[A_{i,pq}]$ is rectangular, it cannot be easily dropped from Eq. (21). Furthermore, the goal is to obtain a linear equation for each mode considered in the frequency range of interest [eliminating matrix $[A_{i,pq}]$ would remove the modal representation in Eq. (21)].

It is important to note that the volume displacement sensor given by Eq. (21) is independent of the excitation frequency and of the type, magnitude, and location of the excitation. Also, the use of polynomial functions to reconstruct the plate response and to design the sensor shape, makes the methodology valid for arbitrary boundary conditions that do not allow rigid modes. It should be noted that since the PVDF film is a strain sensor, it is not sensitive to rigid (whole body) modes.

TABLE III. PVDF film characteristics.

e_{31}	0.046 N/(V m)
e_{32}	0.006 N/(V m)
L_z^s	0.028 mm
μ_x	1.0 cm
μ_y	1.0 cm
Young's modulus (E_{11})	2.0×10^9 Pa
Density (ρ)	1780 kg/m^3

II. EXPERIMENTAL RESULTS

A. Experimental implementation of the volume displacement sensor

The procedure described in Sec. D of Part I was implemented experimentally on the clamped plate described in Table I. Two piezoceramic actuators (a primary ''disturbance'' actuator and a secondary ''control'' actuator) were bonded to the plate. The characteristics and locations of the piezoceramic actuators are described in Table II. The properties of the PVDF film used in the experiments are listed in Table III.

The shapes of the strips were determined using $I=7$ modes for the plate response and polynomial functions of order $R=4$, $S=3$ for the shape functions of the strips in the x and y directions. Once the positions x_{ct} and y_{ct} of the strips have been chosen, the solution of Eq. (21) yields the coefficients of the two PVDF strip shapes which form the volume displacement sensor. The accuracy of the PVDF volume displacement sensor turns out to be quite sensitive to the positions x_{ct} and y_{ct}. This is partly due to the approximation introduced in Eq. (13) to design the shapes of the PVDF strips. Therefore, after fixing the positions of the PVDF strips and solving Eq. (21) for the shape function [$\hat{F}(x)$ and $\hat{F}(y)$] coefficients, Eqs. (12) and (17) are numerically integrated and their sum is compared to the volume displacement measured directly. If the comparison shows that the two curves corresponds well, then the chosen positions x_{ct} and y_{ct} are valid ones. If not, other positions for x_{ct} and y_{ct} have to be tested.

The velocity at a total of 144 (12×12) regularly spaced points on the plate [i.e., $j\omega w(x_{ix},y_{iy})$ for ix and $iy=1$ to 12] was measured using a laser vibrometer. A Bruel & Kjaer analyzer was used to acquire the transfer functions between the excitation signal (to the PZT actuator) and the laser signal. The measured volume displacement can then be evaluated as

$$D_{\text{measured}}=\frac{L_x^{pl}L_y^{pl}}{144}\sum_{ix=1}^{12}\sum_{iy=1}^{12}w(x_{ix},y_{iy}), \tag{22}$$

which is a discrete version of Eq. (7). Figure 3 presents the results for $x_{ct}=0.259$ m and $y_{ct}=0.176$ cm. Figure 3(a) and (b) shows the shapes of the PVDF strips in the x and y direction, respectively. Figure 3(c) presents the comparison of the measured volume displacement (with a laser vibrometer) and the numerically calculated charge response [Eqs. (12) and (17)] of the PVDF sensor when the excitation is induced by the primary actuator. Note, there is no ordinate scale in Fig. 3(b) because the two curves were superposed to facilitate comparison (i.e., the charge response of the PVDF does not have the same unit/scale as the volume displacement response). Figure 3(c) shows an excellent agreement between the numerically calculated signal and the measured volume displacement, which confirms that the chosen positions x_{ct} and y_{ct} are valid. Note that the shapes of the strips [Fig. 3(a), (b)] are almost symmetric. This is intuitively understandable since the experimental mode shapes of the plate to be observed by the PVDF strips are also symmetric (monopole modes).

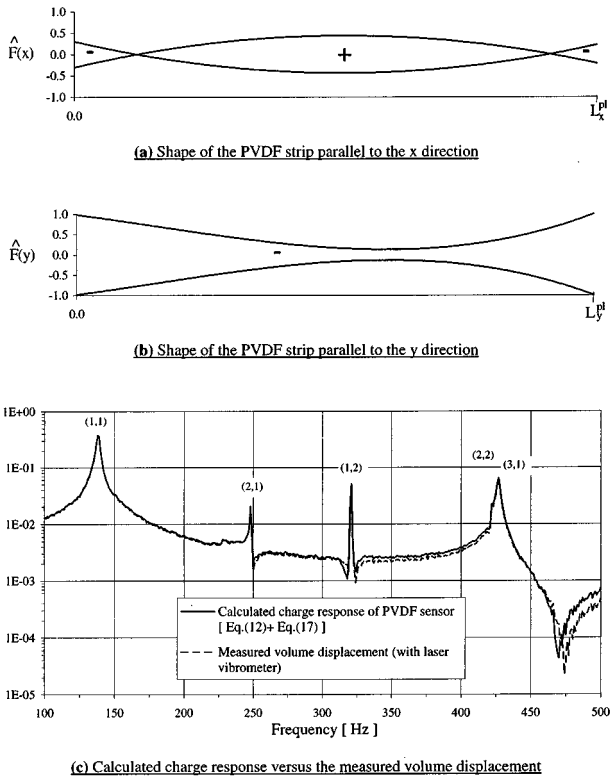

(a) Shape of the PVDF strip parallel to the x direction

(b) Shape of the PVDF strip parallel to the y direction

(c) Calculated charge response versus the measured volume displacement

FIG. 3. Results obtained for the positions $x_{ct}=0.259$ and $y_{ct}=0.176$ m.

The sensor strips shown in Fig. 3(a) and (b) were implemented experimentally and taped to the clamped plate. The total electrical signal from the PVDF sensor (the added signal of the two PVDF strips) was first passed through a preamplifier (with high input impedance and variable gain) and then measured with a Bruel & Kjaer analyzer. Figure 4 and

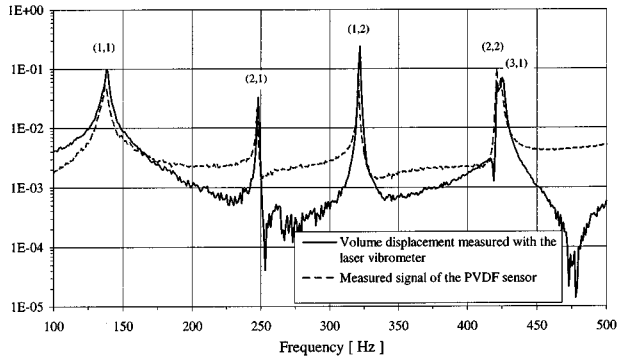

FIG. 4. Performance of sensor when the primary actuator induces the vibrations.

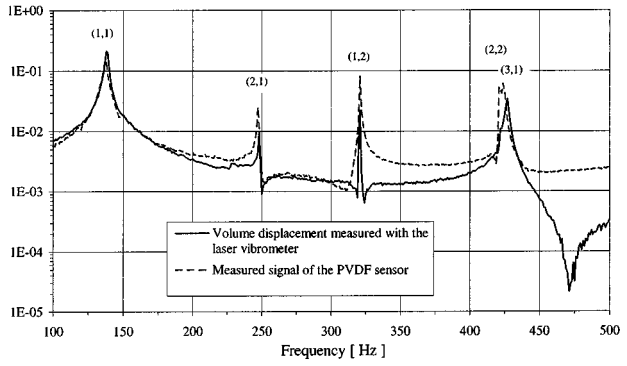

FIG. 5. Performance of sensor when the secondary actuator induces the vibrations.

Fig. 5 present the PVDF sensor signal compared to the direct measurement of the volume displacement when the vibration of the plate is induced by the primary PZT actuator and the secondary PZT actuator respectively. Note that the signal from the PVDF sensor was scaled to be equivalent to the measured volume displacement at 170 Hz. It must be recalled that the sensor is designed using the first seven experimental modes of the plates, so that the contribution of higher order modes is not considered in the shape of the sensor. Thus it is expected that the sensor signal deviates from the volume displacement in higher frequencies. Also, the off-resonance differences between the sensor signal and the measured volume displacement are presumably due to the higher order modes contributions in the flexural strain of the plate. PVDF materials measure strain and are thus more sensitive to higher order modes. In effect, this is more apparent in the case of the primary actuator excitation, which is significantly off-center and thus excites more efficiently the higher order modes of the plate. Note that in both cases the response of the (2,1) and (1,2) modes is large, indicating that these modes have a nonzero volume displacement and are thus not perfectly antisymmetric (this is mainly due to the presence of the PZT on the plate and the imperfections in the experimental boundary conditions). The fact that modes (2,1) and (1,2) have a volume displacement, shows that it is worthwhile to base the design of the sensor from experimentally measured mode shapes (i.e., eigenfunctions). It allows to take into account all the experimental imperfections (i.e., boundary conditions, added mass, added stiffness, plate imperfections, etc.) of the actual experimental setup. The sensor is designed from the measured modal characteristics. Therefore, any modifications of the structure mechanical properties (added mass, stiffness, boundary conditions, etc.) after the design stage will affect the response of the sensor.

B. Active control of volume displacement

This section describes the active control experiment using the volume displacement sensor developed previously. The plate was located in a semi-anechoic chamber for the experiments. Sound pressure levels were measured at nine discrete points equally distributed over a 1.2 m radius from the center of the plate in the plane $x = L_x^{pl}/2$. Note, the main purpose of these sound pressure measurements was to get a good indication of the reduction that could be expected in a realistic application. Therefore, no baffle was installed around the plate. Furthermore, in order to have a single sound pressure value to quantify the reduction obtained by the control, an average sound pressure level in the plane $x = L_x^{pl}/2$ is defined as

$$\langle \tilde{p} \rangle = \frac{R^2}{\rho_0 c_0} \int_{-\pi/2}^{\pi/2} |p(R,\theta)|^2 |\sin(\theta)| d\theta, \tag{23}$$

where R is the radius between the center of the plate and the positions of the measurements point, ρ_0 is the density of air, and c_0 is the speed of sound in air. θ is the angle between the line perpendicular to the plate surface and the line that joins the considered point on the radius R to the center of the plate. Since the sound pressure measurements were done at nine angles θ_i, the discrete version of the last equation is

$$\langle \tilde{p} \rangle = \frac{\pi R^2}{9 \rho_0 c_0} \sum_{i=1}^{9} |p(R,\theta_i)|^2 |\sin(\theta_i)|. \tag{24}$$

The displacement of the plate before and after control was measured using a laser vibrometer at 144 regularly spaced points on the plate surface. The primary actuator was used to induce the unwanted vibration while the secondary actuator was used as the control actuator. The voltage applied on these actuators was typically between 80 and 120 V peak to peak. A feedforward filtered X-LMS controller was used. A number of single frequency was tested (i.e., harmonic control was performed here). The control results are presented for three typical frequencies, two on-resonance and one off-resonance frequency. For each of these frequencies, the measured displacement field as well as the sound pressure levels in the plane $x = L_x^{pl}/2$ are displayed before and after control is applied.

Figure 6 presents the results obtained at 125 Hz, corresponding to an off-resonance frequency of the clamped plate (below the first mode). The structural displacement field before control clearly shows that the plate acts like a monopole type radiator with a maximum displacement close to the primary (i.e., disturbance) actuator location. After control, the plate is forced to act as a dipole type radiator by the secondary (i.e., control) actuator. One can note that the vibration level before and after control are globally the same in this case (the absolute maximum displacement value is approximately 0.08 μm before control, 0.06 μm after control). The experimental sound pressure levels in the plane $x = L_x^{pl}/2$ are shown in Fig. 6(b). The reduction of the average sound pressure level is around 16 dB. This reduction can be attributed solely to the fact that the plate deformation is changed from a monopole type radiator to a dipole type radiator (i.e., modal restructuring[2]). The control of the volume displacement has no appreciable effect on the vibration level at this frequency and only the radiation efficiency, which represents the capacity of the plate the generate sound, is decreased.

Figure 7 presents the results obtained at 140 Hz, which corresponds to the resonance frequency of the first mode, i.e., mode (1,1). As seen in Fig. 7(a), the plate displacement before control corresponds to the (1,1) mode shape, with maximum displacement at the center of the plate. This mode

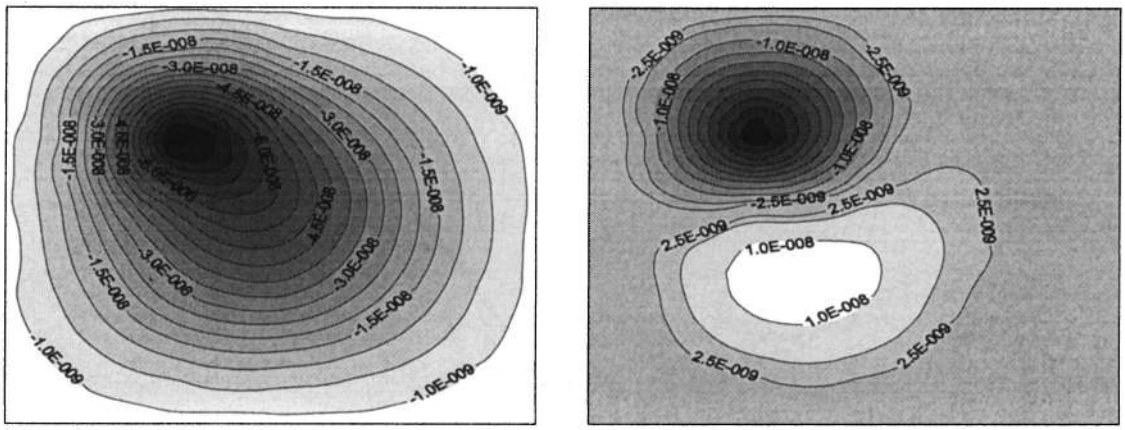

(a) Measured transversal displacements

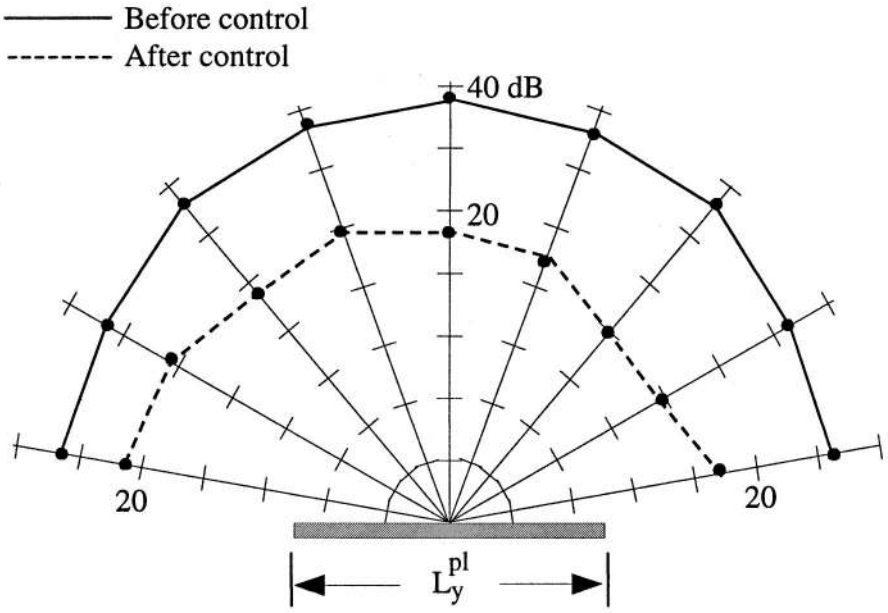

(b) Measured sound pressure levels (plane $x=L_x^{pl}/2$).

FIG. 6. Experimental results at 125 Hz (off-resonance).

is a monopole-type radiator.[2,11] Once again, after control the secondary actuator forces the plate to act as a dipole-type radiator. Note here the vibration levels after control are much lower than before control which indicates that in this case the control combines both vibration restructuring and vibration reduction. Figure 7(b) presents the measured sound pressure levels. The reduction of the average sound pressure level is around 40 dB. The results of the volume displacement control at 140 Hz (Fig. 7) shows that the sound attenuation on resonance of a symmetric mode is associated with a decrease of the radiation efficiency (passage from a monopole type radiator to a dipole-type radiator), combined with a decrease of the vibration amplitudes.

Finally, Fig. 8 presents the results for 320-Hz resonance of mode (1,2). Note that the shape of the displacement after control is globally the same as the one before control. On the other hand, the maximum displacement has been reduced significantly. Therefore, the 14-dB reduction of the average sound pressure level is associated with the reduction of the vibration levels. In this case, the sensor acts as a vibration

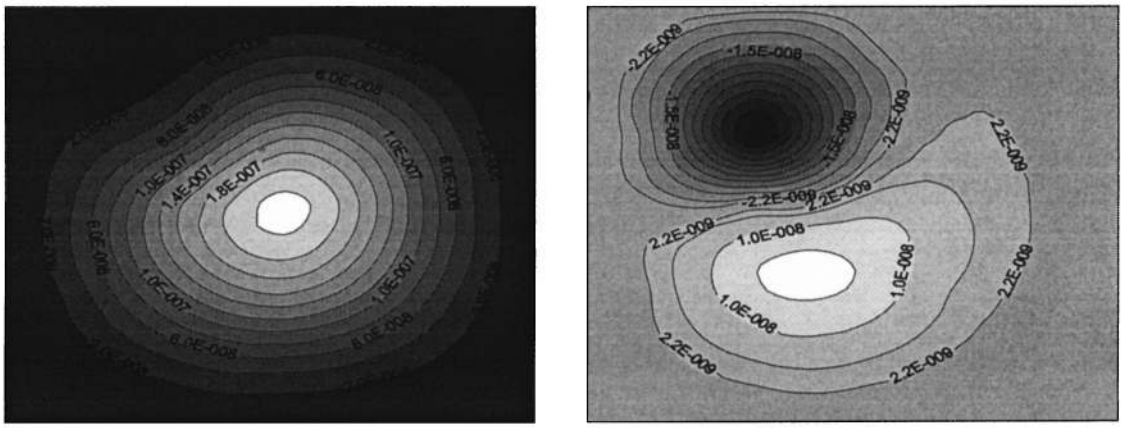

(a) Measured transversal displacements

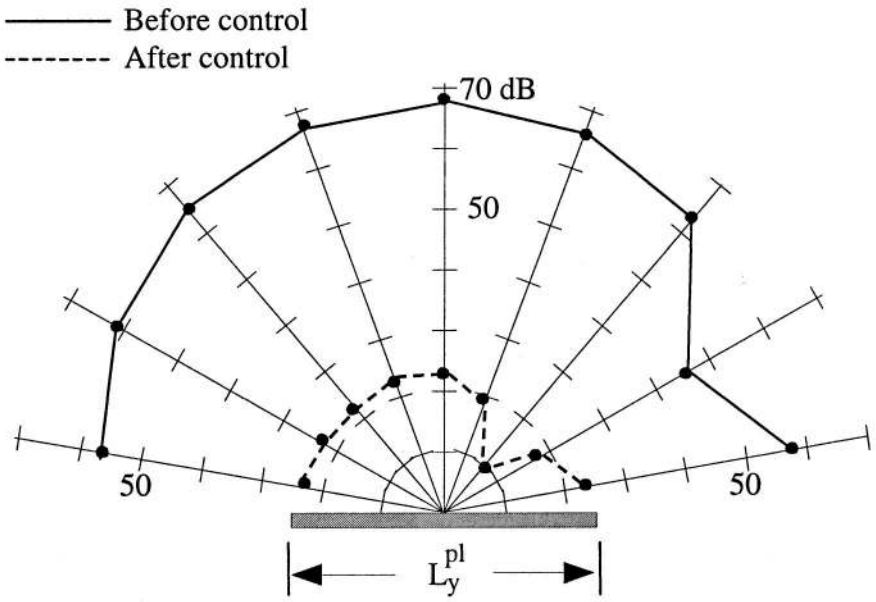

(b) Measured sound pressure levels (plane $x=L_x^{pl}/2$).

FIG. 7. Experimental results at 140 Hz [resonance of mode (1,1)].

sensor, since the plate displacement before control was already a dipole-type radiator. It is interesting to note that the measured pressure directivity in the $x=L_x^{pl}/2$ plane correspond to that of a monopole-type radiator (as expected). At this frequency, it can be deduced from Fig. 8(a) that the pressure directivity in the $y=L_y^{pl}/2$ plane would be that of a dipole-type radiator before and after control. Since the control only reduces the vibrational levels, pressure reductions in the $y=L_y^{pl}/2$ plane are expected to be similar to that measured in the $x=L_x^{pl}/2$ plane.

III. CONCLUSIONS

This paper presents the development of a novel volume displacement sensor for plates and its use in an active control system. The sensor is made of shaped strips of PVDF film in the x and y directions and is independent of the type and frequency of excitation. The approach is very general, since it is based on experimentally determined mode shapes. This allows consideration of any boundary conditions (that do not allow rigid modes), and plates with added punctual mass/

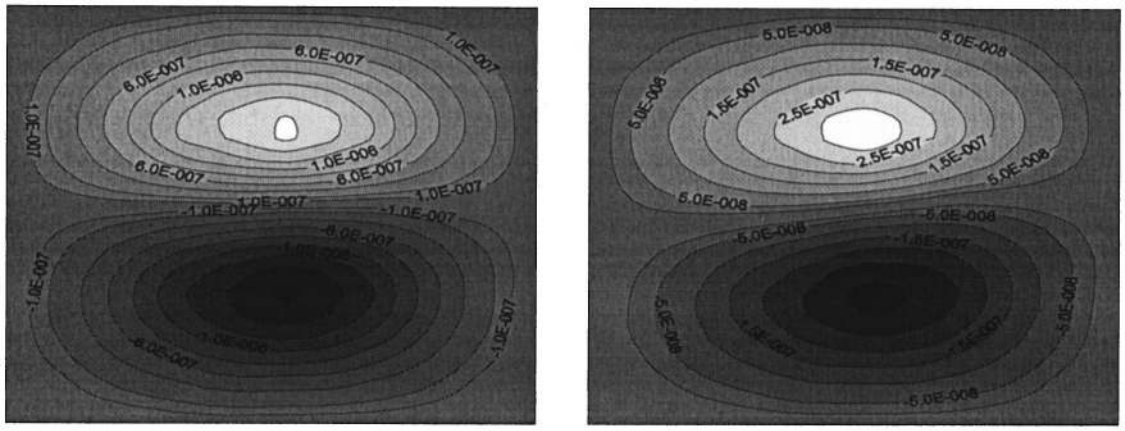

(a) Measured transversal displacements

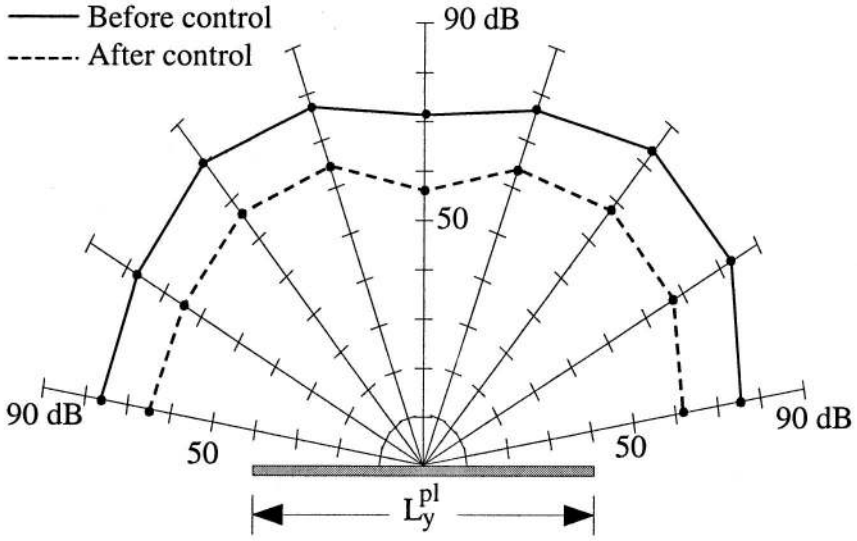

(b) Measured sound pressure levels (plane $x=L_x^{pl}/2$).

FIG. 8. Experimental results at 320 Hz [resonance of mode (1,2)].

stiffness and/or with internal defects. Results were presented for a clamped plate. The sensor was validated by comparing the volume displacement measured with a laser vibrometer to the measured signal from the PVDF sensor. The contribution of high order modes of the plate in the sensor response, as well as the location of the PVDF strips, is sensitive parameters in the sensor design.

A global reduction in the plane $x=L_x^{pl}/2$ of about 16 dB was obtained in the average sound pressure level for the off-resonance frequency case (125 Hz). This reduction is principally associated with a decrease in the radiation efficiency (the plate goes from a monopole-type radiator to a dipole one). For the on resonance case of mode (1,1), at 140 Hz, the obtained reduction in the average sound pressure level is 40 dB. This large reduction for this resonance case is attributed to the fact that the control of volume displacement decreases simultaneously the radiation efficiency and the vibration levels. Finally, for the results at 320 Hz, which correspond to the resonance of mode (1,2), the reduction of 14 dB of the average sound pressure level is associated with the reduction of the vibration levels. In this case, the plate was already acting like a dipole-type radiator before control. Therefore, the controller mainly reduced the vibration levels at this frequency.

The transversal displacement fields and the sound pressure levels obtained experimentally before and after control clearly validates the use of PVDF film directly bonded to a plate as a volume displacement sensors in an active structural

acoustic control (ASAC) system for harmonic excitation. This sensor could be used for ASAC under wide-band excitation if an appropriate digital controller is implemented.

ACKNOWLEDGMENTS

The authors wish to thank Professor Bruno Paillard and his student Martin Bouchard for the development and implementation of the control code on the DSP card. This work was funded in part by the F.C.A.R. (Formation de Chercheurs et l'Aide à la Recherche).

[1] C. R. Fuller, ''Active control of sound transmission/radiation from elastic plates by vibrational inputs: I. Analysis,'' J. Sound Vib. **136**, 1–15 (1990).
[2] C. R. Fuller, S. J. Elliott, and P. A. Nelson, *Active Control of Vibration* (Academic, London, 1996).
[3] C. R. Fuller, C. H. Hansen, and S. D. Snyder, ''Active control of structurally radiated noise using piezoceramic actuator,'' Proceedings of Inter-Noise **89**, 509–511 (1989).
[4] R. L. Clark and C. R. Fuller, ''Experiments on active control of structurally radiated sound using multiple piezoelectric actuators,'' J. Acoust. Soc. Am. **91**, 3313–3320 (1992).
[5] C. K. Lee and F. C. Moon, ''Modal sensors/actuators,'' J. Appl. Mech. **57**, 434–441 (1990).
[6] Y. Gu, R. L. Clark, C. R. Fuller, and A. C. Zander, ''Experiments on active control of plate vibration using piezoelectric actuators and polyvinylidene fluoride (PVDF) modal sensors,'' J. Vib. Acoust. **116**, 303–308 (1994).
[7] R. L. Clark and C. R. Fuller, ''Modal sensing of efficient acoustic radiators with PVDF distributed sensors in active structural acoustic approaches,'' J. Acoust. Soc. Am. **91**, 3321–3329 (1992).
[8] C. Guigou, F. Charette, and A. Berry, ''Active control of finite beam volume velocity using shape PVDF sensor,'' Acta Acust. (China) **82**, 772–783 (1996).
[9] R. L. Clark, R. A. Burdisso, and C. R. Fuller, ''Design approaches for shaping polyvinylidene fluoride sensors in active structural acoustic control (ASAC),'' J. Intell. Mater. Syst. Struct. **4**, 354–365 (1993).
[10] S. D. Snyder, C. H. Hansen, and N. Tanaka, ''Shaped vibration sensors for feedforward control of structural radiation,'' Proceedings of the Second Conference on Recent Advances in Active Control of Sound and Vibration, April 28–30, 1993, Blacksburg, Virginia, pp. 177–188 (1993).
[11] C. E. Wallace, ''Radiation resistance of a rectangular panel,'' J. Acoust. Soc. Am. **51**, 946–952 (1972).
[12] A. Berry, J. L. Guyader, and J. Nicolas, ''A general formulation for the sound radiation from rectangular, baffled plates with arbitrary boundary conditions,'' J. Acoust. Soc. Am. **88**, 2792–2802 (1990).
[13] C. R. Fuller and R. A. Burdisso, ''A wave number domain approach to active control of structure-borne sound,'' J. Sound Vib. **148**, 355–360 (1991).
[14] S. J. Elliott and M. E. Johnson, ''A note on the minimization of the radiated sound power,'' ISVR Technical Memorandum (1992).
[15] M. E. Johnson and S. J. Elliot, ''Active control of sound radiation using volume velocity cancellation,'' J. Acoust. Soc. Am. **98**, 2174–2186 (1995).
[16] J. Rex and S. J. Elliott, ''The QWSIS—A new sensor for structural radiation control,'' 1st International Conference on Motion and Vibration Control Yokohama, pp. 339–343 (1992).
[17] M. E. Johnson and S. J. Elliott, ''Volume velocity sensors for active control,'' Proc. Inst. Acoust. **15**, Part 3, 411–420 (1993).
[18] M. E. Johnson and S. J. Elliott, ''Experiments on the active control of sound radiation using a volume velocity sensor,'' Proceedings of SPIE 1995 conference on Smart Structures and Integrated Systems, Vol. 2443, 658–669 (1995).
[19] C. F. Gerald and P. O. Wheatley, *Applied Numerical Analysis* (Addison-Wesley, New York, 1989).